Supporting Information

3D-Assembled Rutile TiO_2 Spheres with *c*-Channels for Efficient Lithium-Ion Storage

Zhongkai Hao,[a,b] Miao Tian,[a] Yinjuan Ren,[a] Wenrui Dai,[a,b] Meng Wang,[a] Wei Chen[a,b] and Guo Qin Xu[a,b,*]

[a] Department of Chemistry, National University of Singapore, Singapore 117543, Singapore.
[b] National University of Singapore (Suzhou) Research Institute, Suzhou 215123, China.
[*] Corresponding author, Email: chmxugq@nus.edu.sg.

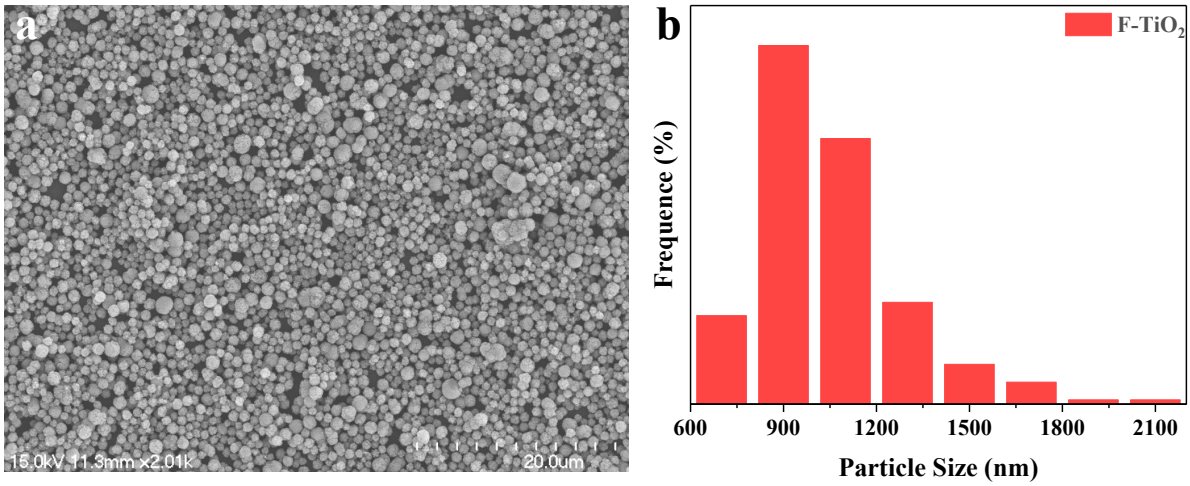

Fig. S1 (a) SEM image and (b) particle size distribution of F-TiO_2 spheres.

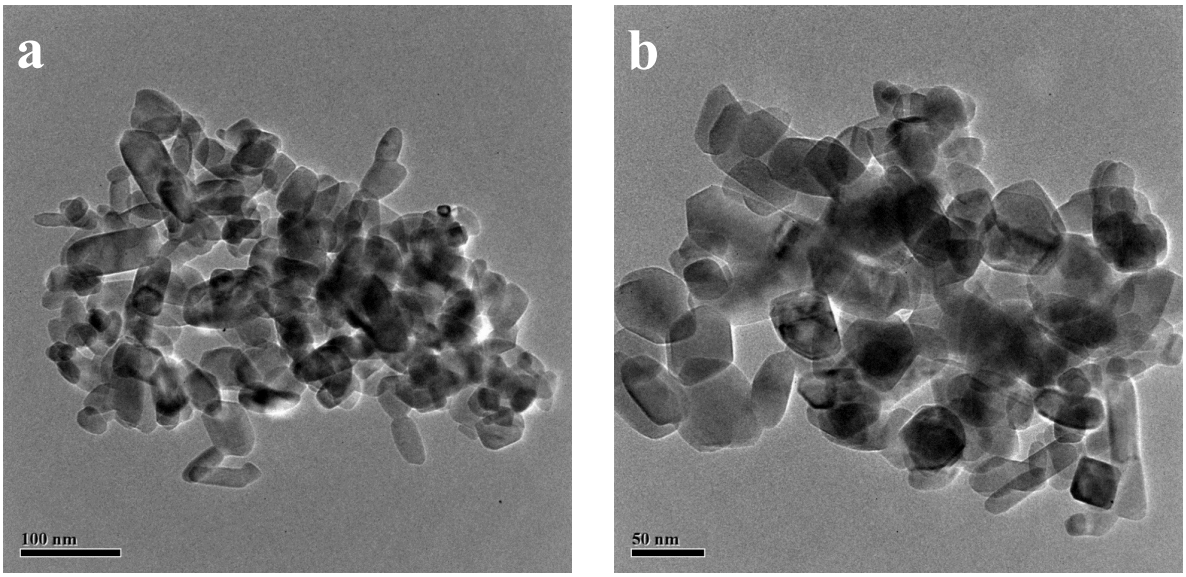

Fig. S2 TEM images of TiO_2 (Rutile) nanoparticles.

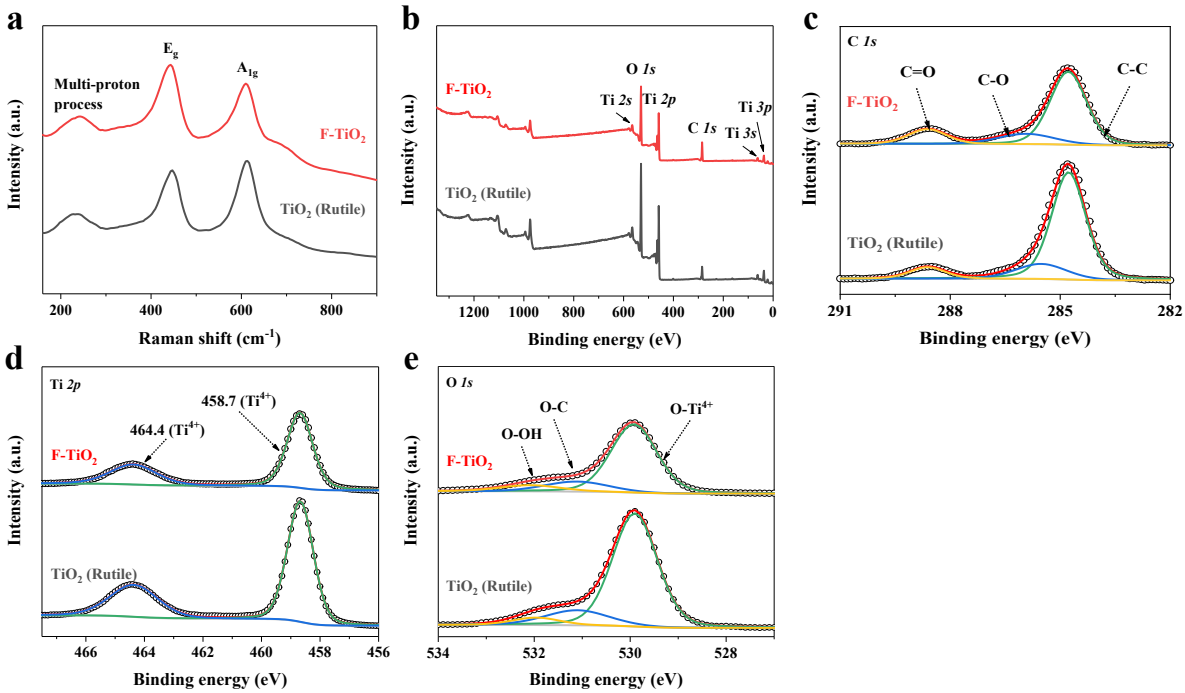

Fig. S3 (a) Raman spectra, (b) Survey XPS spectra, (c,d,e) High-resolution C *1s*, Ti *2p* and O *1s* XPS spectra for F-TiO_2 and TiO_2 (Rutile).

The Raman spectra (Fig. S3a) also manifest that the as-prepared F-TiO_2 possesses the rutile TiO_2 phase according to the characteristic peaks at 243 cm^{-1} (Multi-proton process), 443 cm^{-1} (E_g), and 610 cm^{-1} (A_{1g}).[1,2] From the survey X-ray photoemission spectroscopy (XPS) analysis (Fig. S3b-e), all the peaks, except for C *1s* peak (Fig. S3c), can be assigned to Ti and O elements, indicating the purity of F-TiO_2. Fig. 1d presents the high-resolution Ti *2p* spectra, where two peaks at 458.7 and 464.4 eV are assigned to the Ti $2p_{3/2}$ and Ti $2p_{1/2}$ of Ti^{4+} in TiO_2 lattice, respectively.[3] For the high-resolution O *1s* spectra (Fig. S3e), the XPS curve can be deconvoluted into three peaks, attributable to the O-Ti^{4+}, O-C, and O-OH bonds.[4] Comparing F-TiO_2 with TiO_2 (Rutile), the nearly same peak distribution and positions uncover the identical chemical state of Ti atoms and the fine crystal structure in these samples.[5]

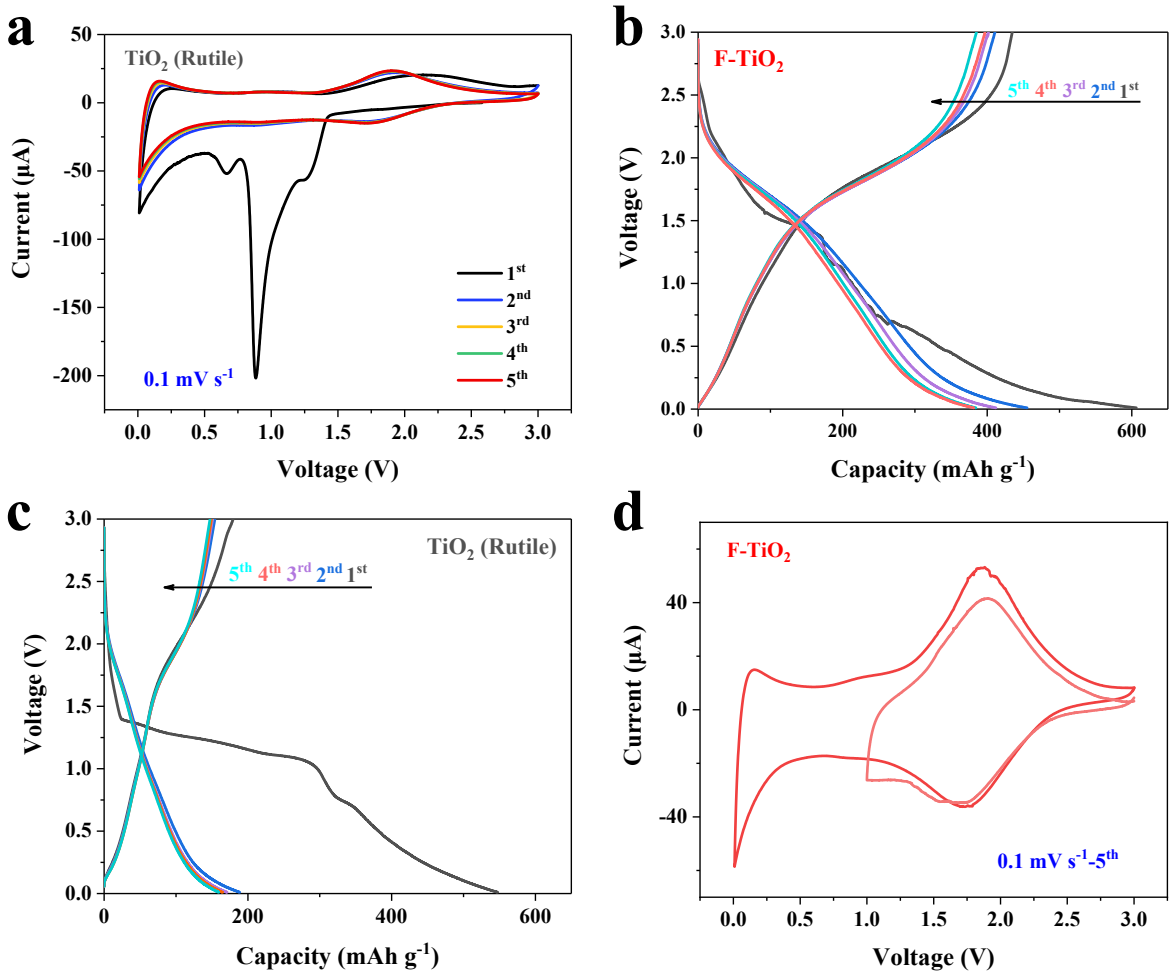

Fig. S4 (a) Cyclic voltammetry (CV) curves of TiO_2 (Rutile) anode at 0.1 mV s^{-1} between 0.01-3 V. The initial five discharge/charge curves of (b) F-TiO_2 and (c) TiO_2 (Rutile) anodes at 0.25 C between 0.01-3 V. (d) the fifth Cyclic voltammetry (CV) curves of TiO_2 (Rutile) anode at 0.1 mV s^{-1}.

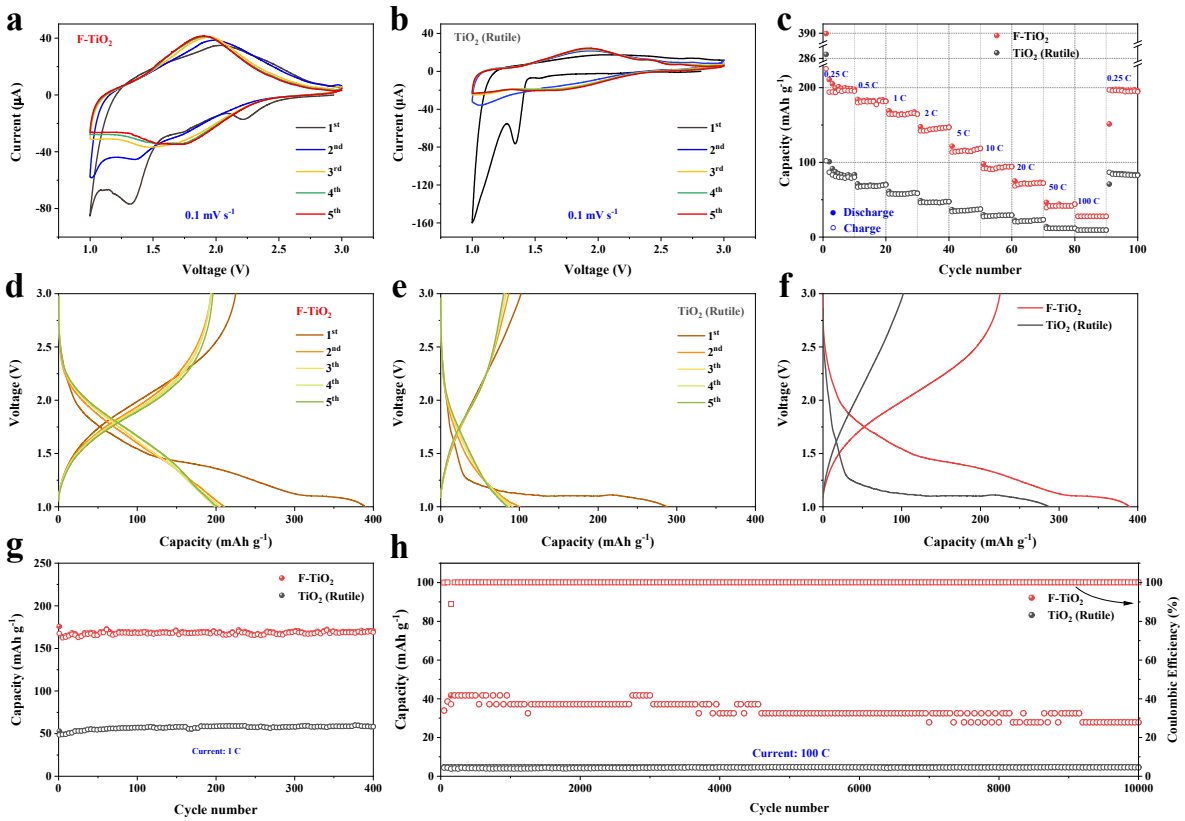

Fig. S5 Cyclic voltammetry (CV) curves of (a) F-TiO_2 and (b) TiO_2 (Rutile) anode at 0.1 mV s^{-1} between 1-3 V. (c) Rate performance of F-TiO_2 and TiO_2 (Rutile) anodes at 0.25-100 C. The initial five discharge/charge curves of (d) F-TiO_2 and (e) TiO_2 (Rutile) anodes at 0.25 C between 1-3 V. (f) The initial discharge/charge curves of F-TiO_2 and TiO_2 (Rutile) anodes at 0.25 C. (g) Cycling performance of F-TiO_2 and TiO_2 (Rutile) anodes at 1 C. (h) Long-term performance and Coulombic efficiency of F-TiO_2 and TiO_2 (Rutile) anodes at 100 C.

The electrochemical behavior of F-TiO_2 and TiO_2 (Rutile) anodes was also investigated between 1-3 V. The CV curves (Fig. S5a-b) show similar peak positions and evolution trends in the redox cycles as that between 0.01-3 V. However, there is an obvious reduction of the current densities in the following cycles.

The lithium storage properties of F-TiO_2 and TiO_2 (Rutile) anodes were evaluated under progressively increased current densities from 0.25 C to 100 C. In Fig. S5c, F-TiO_2 anode exhibits the better rate capacities at all the current densities in comparison with TiO_2 (Rutile) anode. Reversible capacities about 196, 181, 164, 144, 116, 92, 71, 42, 28 mAh g^{-1} are delivered at 0.25, 0.5, 1, 2, 5, 10, 20, 50, and 100 C, respectively. And a specific capacity about 196 mAh g^{-1} remains once the current density returned to 0.25 C, indicating the remarkable reversibility

of F-TiO_2 anode. The corresponding values for TiO_2 (Rutile) are only 80, 68, 57, 46, 35, 28, 21, 11, 9.3 and 83 mAh g^{-1}. It is also noteworthy that the initial discharge/charge capacities of F-TiO_2 anode at 0.25 C are 390 and 225 mAh g^{-1}, giving an initial Coulombic efficiency about 58% (Fig. S5d,f). The initial capacity loss in the first discharge/charge cycle is mainly due to the irreversible reactions between TiO_2 nanoparticles and the electrolyte. On the other hand, TiO_2 (Rutile) anode only affords the initial lithiation and delithiation capacities about 287 and 102 mAh g^{-1}, respectively, with a much lower Coulombic efficiency of 36% (Fig. S5e,f), in line well the results discussed in the CV measurement.

Fig. S5g presents the cycling performance of F-TiO_2 and TiO_2 (Rutile) anodes at 1 C. F-TiO_2 anode maintains a reversible capability of 162 mAh g^{-1} after 400 cycles while TiO_2 (Rutile) anode only gives a value of 61 mAh g^{-1}. The long-term cycling stability of F-TiO_2 and TiO_2 (Rutile) anodes was further examined under higher current density. At the current rate of 100 C (Fig. S5h), F-TiO_2 anode has a specific capacity about 28 mAh g^{-1} after 10 000 cycles with a Coulombic efficiency near 100%, but a much lower value of 4.6 mAh g^{-1} for TiO_2 (Rutile) anode. These results clearly imply the vital role of 3D architecture with radially organized nanorods (*c*-Channels) for the improved electrochemical performance of F-TiO_2 anode in Li-ion batteries.

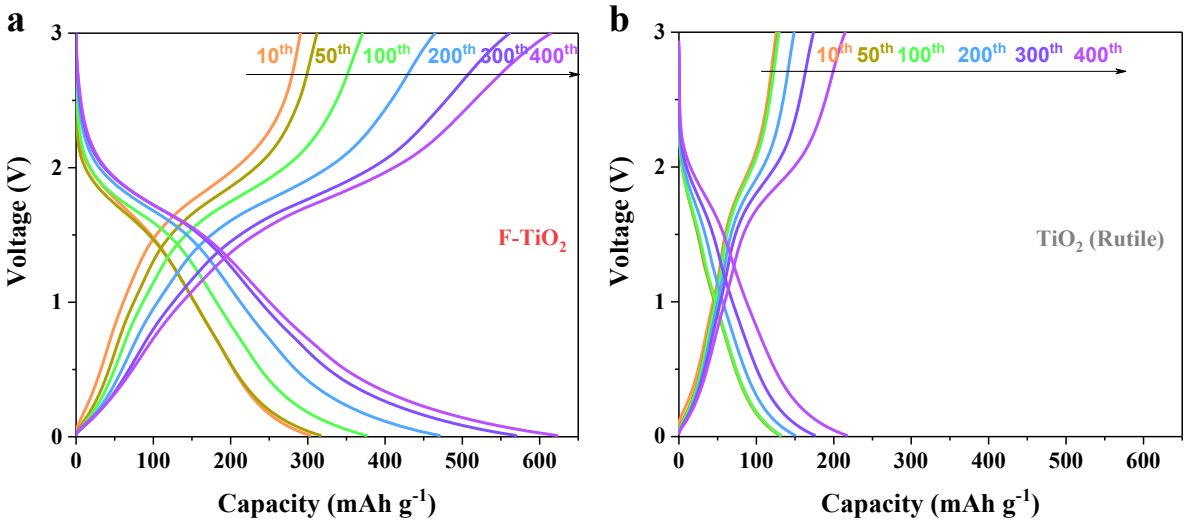

Fig. S6 Different galvanostatic discharge/charge cycling profiles of (a) F-TiO_2 and (b) TiO_2 (Rutile) anodes at 1 C.

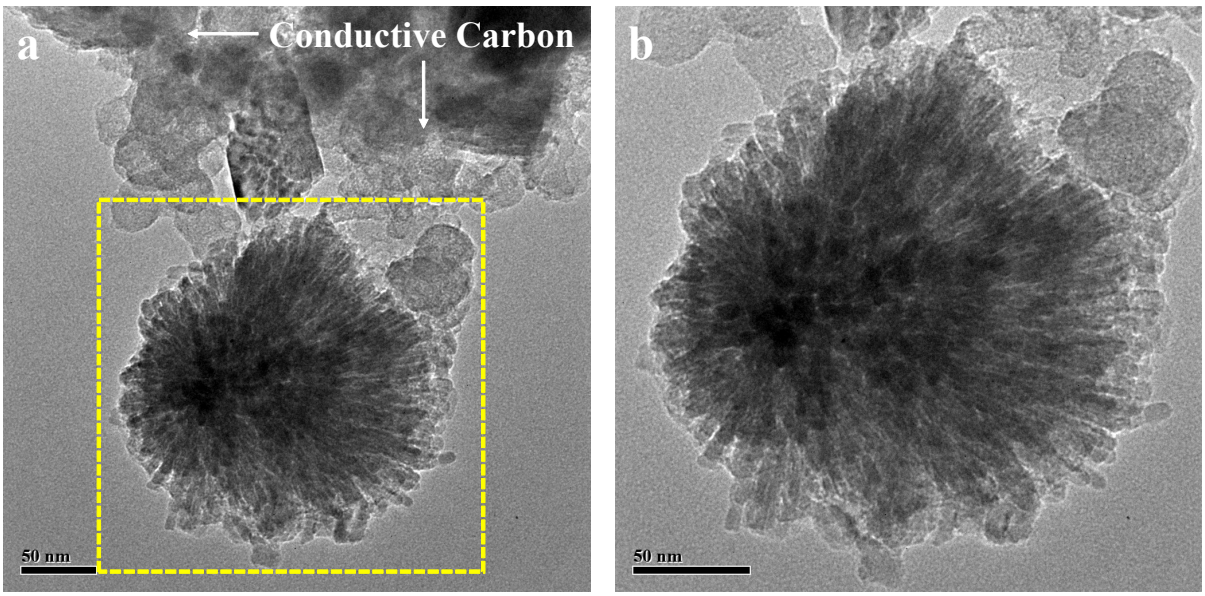

Fig. S7 TEM images of F-TiO_2 spheres after 400 discharge/charge cycles at 1 C.

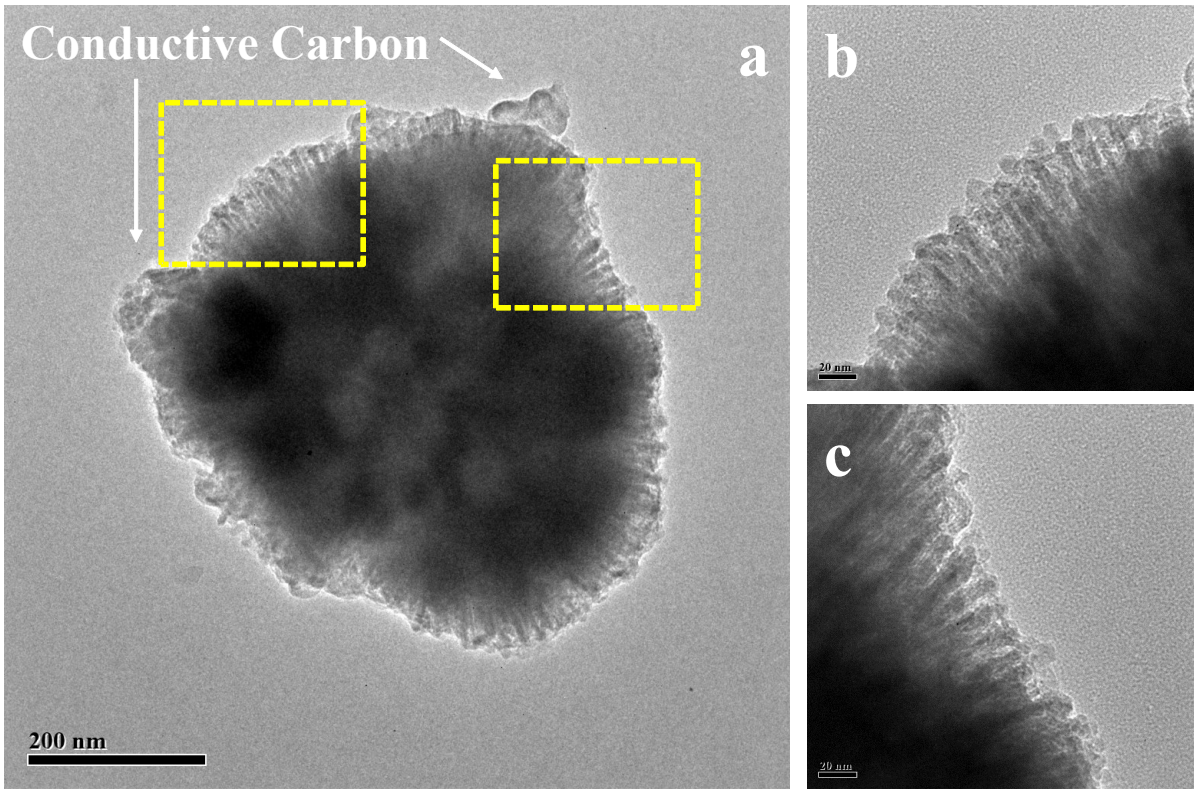

Fig. S8 TEM images of F-TiO_2 spheres after 10 000 discharge/charge cycles at 100 C.

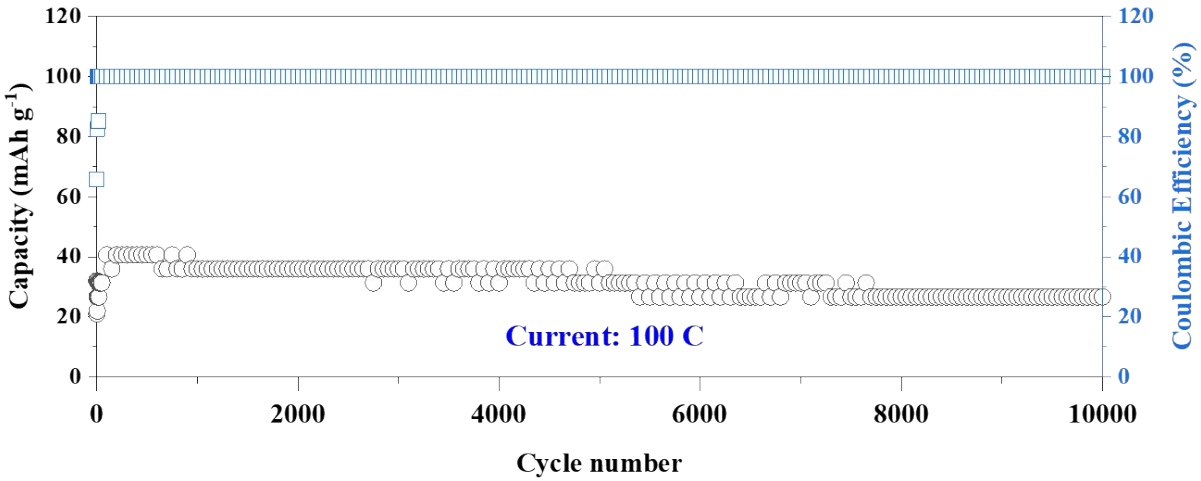

Fig. S9 Long-term performance and Coulombic efficiency of TiO_2 (Rutile) anode at 100 C.

Table S1 Cyclability and rate capability comparison of F-TiO_2 electrode vs. other reported representative TiO_2-based anodes in Lithium-ion batteries.

Materials	Rate capability (mAh g^{-1})	Cycling capacity (mAh g^{-1})	Reference
F-TiO_2	385 at 0.25 C 326 at 0.5 C 296 at 1 C (168 mA g^{-1}) 270 at 2 C 223 at 5 C 187 at 10 C 152 at 20 C 105 at 50 C 70 at 100 C	335 after 70 cycles at 1 C 615 after 400 cycles at 1 C 386 after 400 cycles at 2 C 67 after 10 000 cycles at 100 C	This work
Oxygen-deficient $TiO_{2-\delta}$ nanoparticles	(1 C = 336 mA g^{-1})	131 after 20 cycles at 1 C 130 after 20 cycles at 10 C	6
Black anatase TiO_2	(1 C = 200 mA g^{-1})	188 after 100 cycles at 0.2 C 105 after 100 cycles at 100 C	7
B-$TiO_{2-\delta}$	256 at 0.25 C 214 at 0.5 C 178 at 1 C (168 mA g^{-1}) 156 at 2 C 119 at 5 C 96 at 10 C 77 at 20 C 62 at 50 C 50 at 100 C	335 after 500 cycles at 1 C 50 after 10 000 cycles at 100 C	8
Nanometer-sized rutile TiO_2	168 at 0.05 C 150 at 0.2 C 132 at 1 C (168 mA g^{-1}) 110 at 5 C 100 at 10 C 81 at 20 C 70 at 30 C	160 after 50 cycles at 0.05 C	9
Octahedral TiO_2 nanocages	(1 C = 170 mA g^{-1})	140 after 200 cycles at 0.5 C 110 after 200 cycles at 1 C	10
TiO_2 hollow sphere	145 at 1 C (173 mA g^{-1}) 127 at 2 C 120 at 5 C 106 at 10 C 81 at 20 C 61 at 40 C	148 after 300 cycles at 1 C	11
Mesoporous TiO_2 hollow spheres	196 at 1 C (173 mA g^{-1}) 165 at 5 C 127 at 10 C 76 at 20 C 49 at 30 C	128 after 1000 cycles at 10 C	12
Mesoporous yolk–shell anatase TiO_2/TiO_2(B) microspheres	182 at 40 C (1 C = 168 mA g^{-1})	260 after 500 cycles at 1 C	13
Hollow anatase TiO_2	196 at 1 A g^{-1}	195 after 500 cycles at 0.1 A g^{-1}	14
3D porous TiO_2 with c-channel	190 at 0.2 C (1 C = 168 mA g^{-1})	150 after 300 cycles at 0.5 C 140 after 300 cycles at 2 C 120 after 300 cycles at 5 C	15
Hydrogenated anatase TiO_2	289 at 0.2 C 105 at 20 C	200 after 200 cycles at 1 C	16

	(1 C = 168 mA g^{-1})		
Hollow TiO_{2-x} porous microspheres	222 at 0.5 C 192 at 1 C (190 mA g^{-1}) 121 at 5 C 92 at 10 C	151 after 300 cycles at 1 C	17
Hydrogenated oxygen-deficient blue anatase	196 at 0.5 C 175 at 1 C (336 mA g^{-1})	186 after 100 cycles at 0.5 C	18
Blue TiO_2 with oxygen deficiency	300 at 0.2 C (1 C = 168 mA g^{-1})	165 after 100 cycles at 1 C	19
Blue TiO_2	200 at 0.05 C 129 at 5 C (1 C = 336 mA g^{-1})	180 after 100 cycles at 0.05 C	20
Electrospun $TiO_{2-\delta}$ Nanofibers	N. A.	181 after 500 cycles at 0.15 A g^{-1}	21
Surface-amorphized TiO_2 nanocrystals	175 at 1C (335 mA g^{-1}) 164 at 10C 120 at 50C	131 after 500 cycles at 1 C	22
am-TiO_2/G-60	187 at 0.25 C 122 at 100 C (1 C = 168 mA g^{-1})	130 after 5000 cycles at 10 C 110 after 20 000 cycles at 50 C	23
am-TiO_2	(1 C = 335 mA g^{-1})	200 after 50 cycles at 0.1 C 125 after 50 cycles at 10 C	24
am-TiO_2 thin film on carbon nanotubes	N. A.	240 after 10 cycles at 0.1 A g^{-1} 120 after 1000 cycles at 10 A g^{-1}	25
am-TiO_2/G	N. A.	200 after 50 cycles at 0.04 A g^{-1} 120 after 500 cycles at 1 A g^{-1} 100 after 500 cycles at 2 A g^{-1}	26
am-TiO_2 thin film on graphene nanosheets	150 at 0.1 A g^{-1} 135 at 0.2 A g^{-1} 125 at 0.4 A g^{-1} 100 at 0.8 A g^{-1} 95 at 1.2 A g^{-1}	140 after 100 cycles at 0.1 A g^{-1}	27
am-TiO_2 nanotubes	229 at 1 A g^{-1} 123 at 50 A g^{-1}	170 after 100 cycles at 10 A g^{-1} 140 after 100 cycles at 30 A g^{-1}	28
am-TiO_2 nanotube arrays	200 at 1.2 C 150 at 12 C 80 at 96 C	110 after 2000 cycles at 1.2 C	29

N.A.: Not available

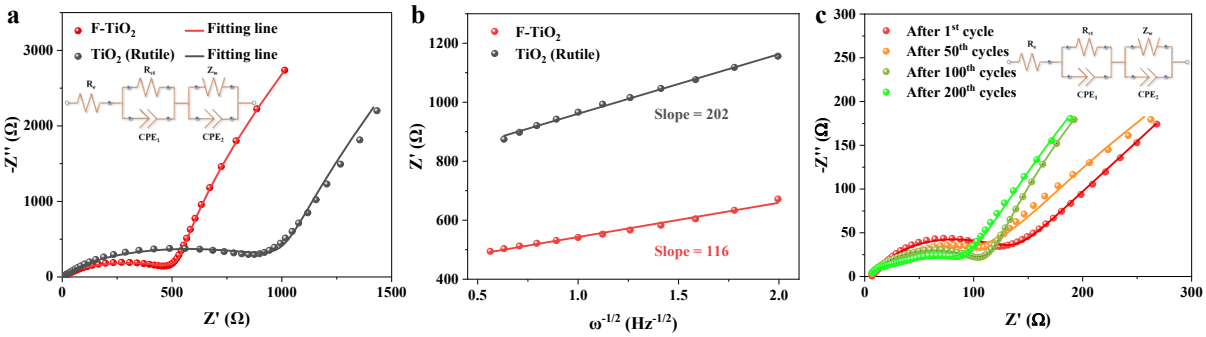

Fig. S10 (a) Nyquist plots of F-TiO_2 and TiO_2 (Rutile) anodes at room temperature. The inset is the corresponding equivalent circuit. (b) The plots about Z' versus $\omega^{-1/2}$ in the low-frequency region. (c) Nyquist plots of F-TiO_2 anode after different cycles at 1 C.

The ion diffusion coefficient (D_0) can be inferred from the following equations:[30,31]

$$Z' = R_1 + R_{ct} + \sigma\omega^{-\frac{1}{2}} \qquad (1)$$

$$D_0 = 0.5\left(\frac{RT}{nAF^2\sigma C}\right)^2 \qquad (2)$$

where R is the gas constant; T is the absolute temperature; n is the electronic transport ratio during the redox process; A is the working area of the electrode; F is the Faraday constant; σ is the slope on the diffusion state of EIS measurement; C is the molar density of Li ions in an electrode.

Table S2 Equivalent circuit parameters used to simulate the EIS data of F-TiO_2 and TiO_2 (Rutile) anodes before and after different cycles.

	R_e (Ω)	R_{ct} (Ω)	σ (Ω cm^2 s$^{-1/2}$)	D_0 (cm^2 s^{-1})
TiO_2 (Rutile)	1.82	1033	202	6.80×10^{-13}
F-TiO_2	2.76	543	116	2.06×10^{-12}
After 1st cycle	6.09	140	-	-
After 50th cycles	2.54	135	-	-
After 100th cycles	3.26	116	-	-
After 200th cycles	1.00	111	-	-

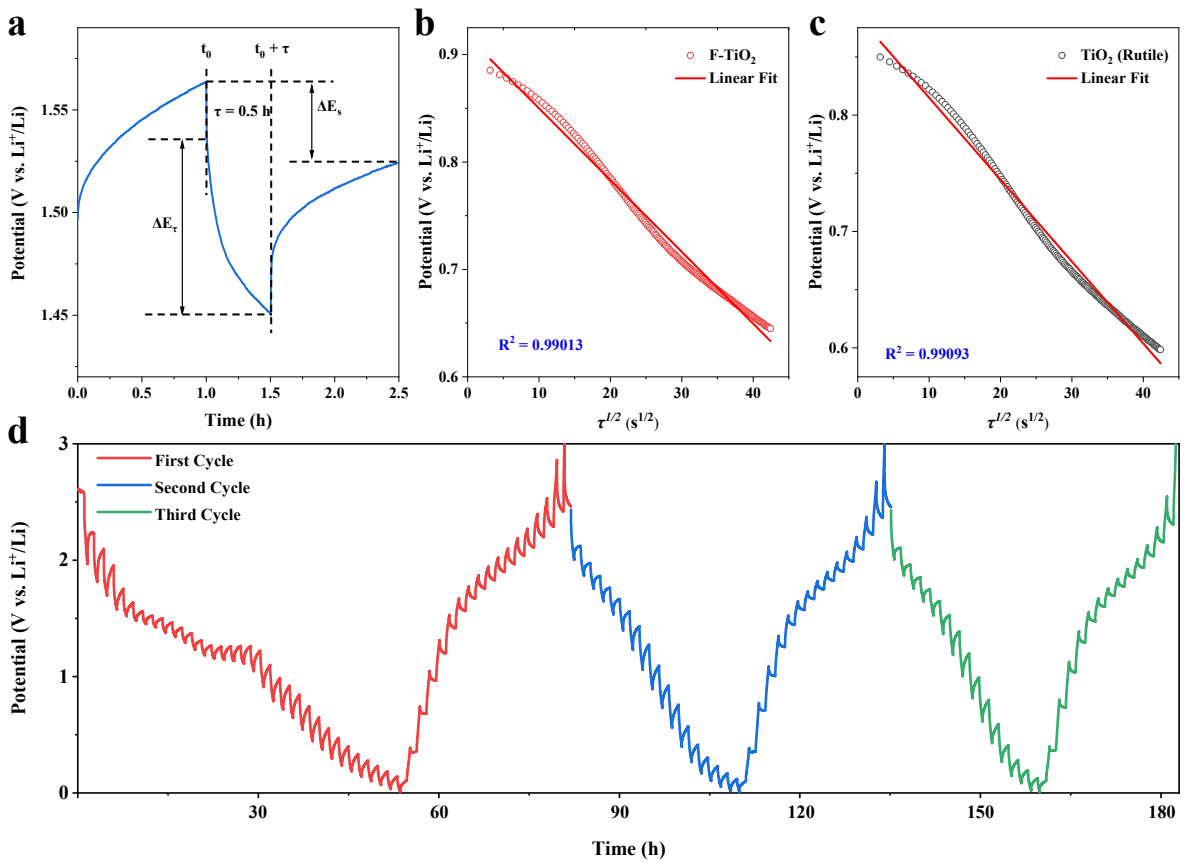

Fig. S11 (a) Current step diagram at 1.50 V of F-TiO_2 anode. (b) Linear behavior of the potential vs. $\tau^{1/2}$ in GITT at 0.90 V of F-TiO_2 anode in the first lithiation process. (c) Linear behavior of the potential vs. $\tau^{1/2}$ in GITT at 0.89 V of TiO_2 (Rutile) anode in the first lithiation process. (d) Three charge/discharge profiles in GITT test of F-TiO_2 anode.

The values of the resulting lithium ion diffusion coefficient (D_{Li^+}) in the lithiation reactions can be estimated from the GITT curves by the following formula (3):[32]

$$D_{Li^+} = \frac{4}{\pi}\left(\frac{mV_M}{MS}\right)^2\left(\frac{\Delta Es}{\tau(d\Delta E\tau/d\sqrt{\tau})}\right)^2 \left(\tau \ll L^2/D_{Li}^{+}\right) \qquad (3)$$

where τ is the duration of the current pulse; m is the mass of the active electrode material; V_M is the molar volume of the active material; M_B is the molar mass of the active material; S is the geometric area of the electrode; ΔE_s is the quasi-thermodynamic equilibrium potential difference before and after the current pulse; ΔE_τ is the potential difference during current pulse. As the potential profiles are linearly proportional to $\tau^{1/2}$ for F-TiO_2 and TiO_2 (Rutile) anodes (Fig. S11b,c), the diffusion coefficient (D_{Li^+}) can be calculated from the following simplified equation (4):

$$D_{Li^+} = \frac{4}{\pi\tau}\left(\frac{mV_M}{MS}\right)^2\left(\frac{\Delta Es}{\Delta E\tau}\right)^2 \qquad (4)$$

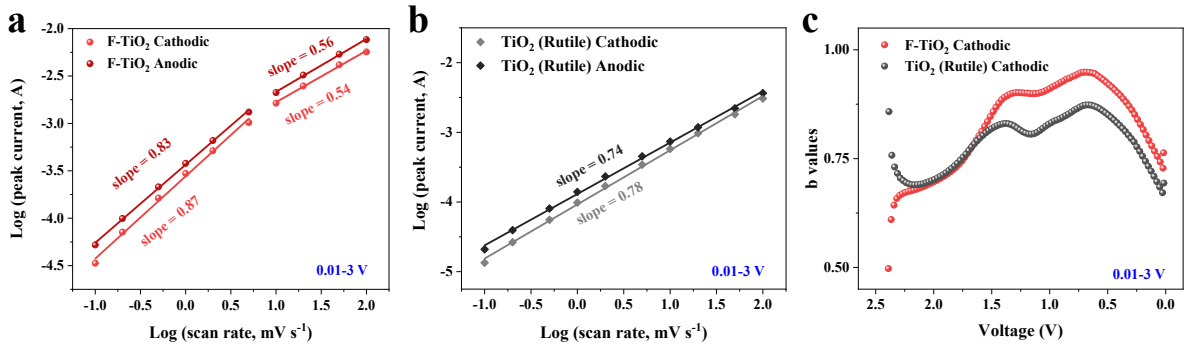

Fig. S12 b-value analysis of (a) F-TiO_2 and (b) TiO_2 (Rutile) anodes between 0.01-3 V. (c) Comparison of b-values for F-TiO_2 and TiO_2 (Rutile) anodes between 0.01-3 V.

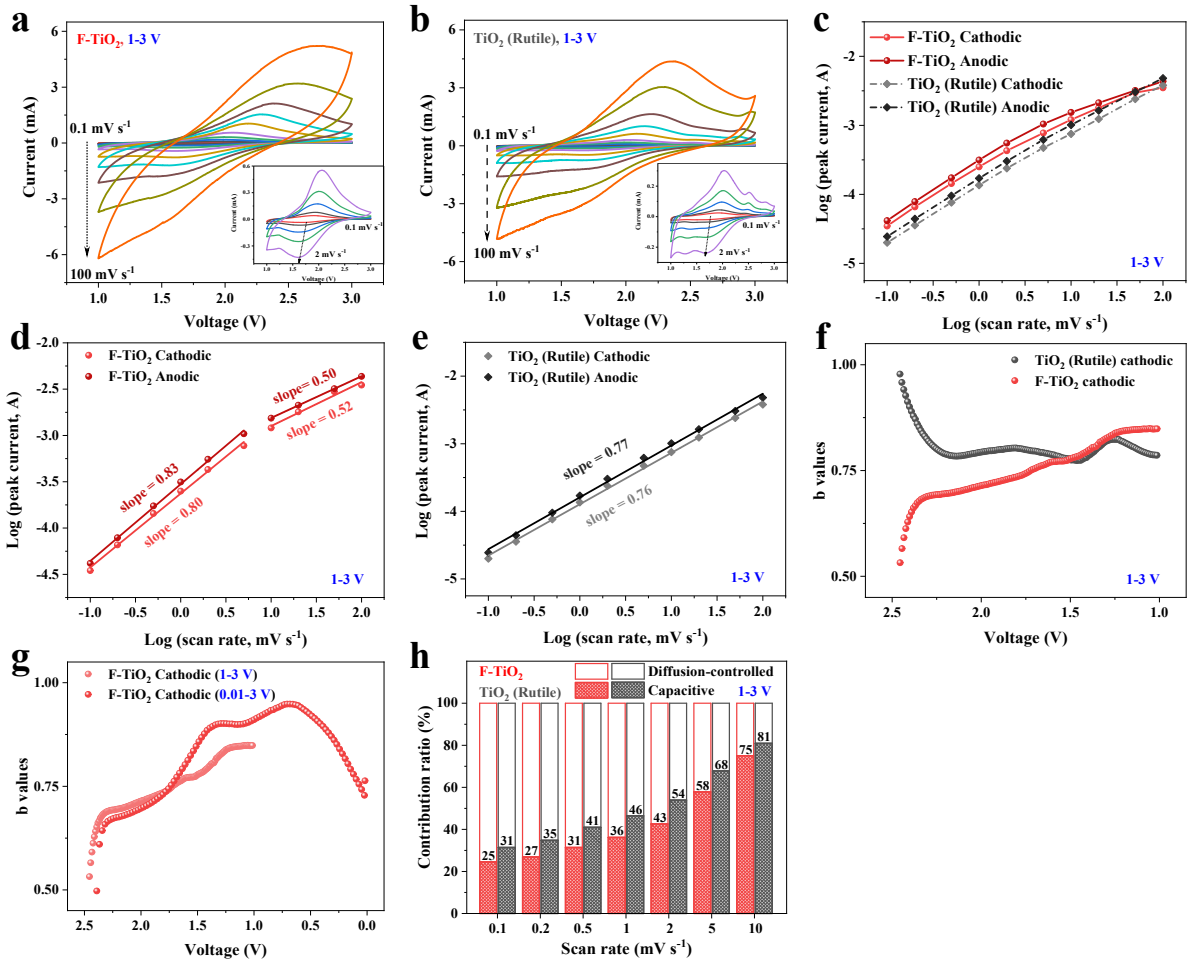

Fig. S13 (a,b) CV curves at different scan rates from 0.1 to 100 mV s^{-1}, and (c,d,e) b-value analysis using the relationship between the peak current and the scan rate between 1-3 V. (f,g) Comparison of b-values for F-TiO_2 and TiO_2 (Rutile) anodes between 1-3 V and 0.01-3 V. (h) Comparation of capacitive and diffusion-controlled capacities between 1-3 V.

References

1. J. Lin, Y. U. Heo, A. Nattestad, M. Shahabuddin, Y. Yamauchi and J. H. Kim, *Phys. Chem. Chem. Phys.*, 2015, **17**, 7208-7213.
2. D. McNulty, E. Carroll and C. O'Dwyer, *Adv. Energy Mater.*, 2017, **7**, 1602291.
3. D. O. Scanlon, C. W. Dunnill, J. Buckeridge, S. A. Shevlin, A. J. Logsdail, S. M. Woodley, C. R. Catlow, M. J. Powell, R. G. Palgrave, I. P. Parkin, G. W. Watson, T. W. Keal, P. Sherwood, A. Walsh and A. A. Sokol, *Nat. Mater.*, 2013, **12**, 798-801.
4. G. Ketteler, S. Yamamoto, H. Bluhm, K. Andersson, D. E. Starr, D. F. Ogletree, H. Ogasawara, A. Nilsson and M. Salmeron, *J. Phys. Chem. C*, 2007, **111**, 8278-8282.
5. L. Li, J. Yan, T. Wang, Z. J. Zhao, J. Zhang, J. Gong and N. Guan, *Nat. Commun.*, 2015, **6**, 5881.
6. J.-Y. Shin, J. H. Joo, D. Samuelis and J. Maier, *Chem. Mater.*, 2012, **24**, 543-551.
7. S.-T. Myung, M. Kikuchi, C. S. Yoon, H. Yashiro, S.-J. Kim, Y.-K. Sun and B. Scrosati, *Energy Environ. Sci.*, 2013, **6**, 2609-2614.
8. Z. Hao, Q. Chen, W. Dai, Y. Ren, Y. Zhou, J. Yang, S. Xie, Y. Shen, J. Wu, W. Chen and G. Q. Xu, *Adv. Energy Mater.*, 2020, **10**, 1903107.
9. Y. S. Hu, L. Kienle, Y. G. Guo and J. Maier, *Adv. Mater.*, 2006, **18**, 1421-1426.
10. Z. Wang and X. W. Lou, *Adv. Mater.*, 2012, **24**, 4124-4129.
11. G. Zhang, H. B. Wu, T. Song, U. Paik and X. W. Lou, *Angew. Chem. Int. Ed.*, 2014, **53**, 12590-12593.
12. B. Y. Guan, L. Yu, J. Li and X. W. D. Lou, *Sci. Adv.*, 2016, **2**, e1501554.
13. H. Wei, E. F. Rodriguez, A. F. Hollenkamp, A. I. Bhatt, D. Chen and R. A. Caruso, *Adv. Funct. Mater.*, 2017, **27**, 1703270.
14. D. H. Lee, B. H. Lee, A. K. Sinha, J. H. Park, M. S. Kim, J. Park, H. Shin, K. S. Lee, Y. E. Sung and T. Hyeon, *J. Am. Chem. Soc.*, 2018, **140**, 16676-16684.
15. J. Baek, S. Park, C. K. Song, T. Y. Kim, I. Nam, J. M. Lee, J. W. Han and J. Yi, *Chem. Commun.*, 2015, **51**, 15019-15022.
16. J. Zheng, L. Liu, G. Ji, Q. Yang, L. Zheng and J. Zhang, *ACS Appl. Mater. Interfaces*, 2016, **8**, 20074-20081.
17. C. Wang, F. Wang, Y. Zhao, Y. Li, Q. Yue, Y. Liu, Y. Liu, A. A. Elzatahry, A. Al-Enizi, Y. Wu, Y. Deng and D. Zhao, *Nano Research*, 2016, **9**, 165-173.
18. J. Zheng, Y. Liu, G. Ji, P. Zhang, X. Cao, B. Wang, C. Zhang, X. Zhou, Y. Zhu and D. Shi, *ACS Appl. Mater. Interfaces*, 2015, **7**, 23431-23438.
19. J. Zheng, G. Ji, P. Zhang, X. Cao, B. Wang, L. Yu and Z. J. Xu, *Chem. Eur. J.*, 2015, **21**, 18309-18315.
20. J. Qiu, S. Li, E. Gray, H. Liu, Q. F. Gu, C. Sun, C. Lai, H. Zhao and S. Zhang, *J. Phys. Chem. C*, 2014, **118**, 8824-8830.
21. J. Sundaramurthy, V. Aravindan, P. Suresh Kumar, S. Madhavi and S. Ramakrishna, *J. Phys. Chem. C*, 2014, **118**, 16776-16781.
22. T. Xia, W. Zhang, J. Murowchick, G. Liu and X. Chen, *Nano Lett.*, 2013, **13**, 5289-5296.
23. J. Han, A. Hirata, J. Du, Y. Ito, T. Fujita, S. Kohara, T. Ina and M. Chen, *Nano Energy*, 2018, **49**, 354-362.
24. W. J. H. Borghols, D. Lützenkirchen-Hecht, c. W. C. Ullrich Haake, U. Lafont, E. M. Kelder, E. R. H. v. Eck, A. P. M. Kentgens, F. M. Mulder and M. Wagemaker, *J. Electrochem. Soc.*, 2010, **157**, A582-A588.
25. M. Xie, X. Sun, C. Zhou, A. S. Cavanagh, H. Sun, T. Hu, G. Wang, J. Lian and S. M. George, *J. Electrochem. Soc.*, 2015, **162**, A974-A981.

26. C. Ban, M. Xie, X. Sun, J. J. Travis, G. Wang, H. Sun, A. C. Dillon, J. Lian and S. M. George, *Nanotechnology*, 2013, **24**, 424002.
27. M. Li, X. Li, W. Li, X. Meng, Y. Yu and X. Sun, *Electrochem. Commun.*, 2015, **57**, 43-47.
28. H. T. Fang, M. Liu, D. W. Wang, T. Sun, D. S. Guan, F. Li, J. Zhou, T. K. Sham and H. M. Cheng, *Nanotechnology*, 2009, **20**, 225701.
29. A. Lamberti, N. Garino, A. Sacco, S. Bianco, A. Chiodoni and C. Gerbaldi, *Electrochim. Acta*, 2015, **151**, 222-229.
30. C. Ho, I. D. Raistrick and R. A. Huggins, *J. Electrochem. Soc.*, 1980, **127**, 343-350.
31. H. Huang, S. Gao, A.-M. Wu, K. Cheng, X.-N. Li, X.-X. Gao, J.-J. Zhao, X.-L. Dong and G.-Z. Cao, *Nano Energy*, 2017, **31**, 74-83.
32. W. Weppner and R. A. Huggins, *J. Electrochem. Soc.*, 1977**, 124**, 1569-1578.